Available online at www.sciencedirect.com
SCIENCE DIRECT®
Comput. Methods Appl. Mech. Engrg. 193 (2004) 933–951
Computer methods in applied mechanics and engineering
www.elsevier.com/locate/cma

Reproducing kernel element method. Part I: Theoretical formulation

Wing Kam Liu [a,*], Weimin Han [b], Hongsheng Lu [a], Shaofan Li [c], Jian Cao [a]

[a] Department of Mechanical Engineering, Northwestern University, The Technological Institute, 2145 Sheridan Road, Evanston, IL 60208-3111, USA
[b] Department of Mathematics, University of Iowa City, IA 52242, USA
[c] Department of Civil and Environmental Engineering, University of California, Berkeley, CA 94720, USA

Received 8 April 2003; received in revised form 10 July 2003; accepted 4 December 2003

Abstract

In this paper and its sequels, we introduce and analyze a new class of methods, collectively called the reproducing kernel element method (RKEM). The central idea in the development of the new method is to combine the strengths of both finite element methods (FEM) and meshfree methods. Two distinguished features of RKEM are: the arbitrarily high order smoothness and the interpolation property of the shape functions. These properties are desirable especially in solving Galerkin weak forms of higher order partial differential equations and in treating Dirichlet boundary conditions. So unlike the FEM, there is no need for special treatment with the RKEM in solving high order equations. Compared to meshfree methods, Dirichlet boundary conditions do not present any difficulty in using the RKEM. A rigorous error analysis and convergence study of the method are presented. The performance of the method is illustrated and assessed through some numerical examples.

Keywords: Approximation theory; Finite element method; Meshfree method; Reproducing kernel element method

1. Introduction

Interests in constructing versatile finite element interpolants, meshfree interpolants, or general partition of unity shape functions is the current trend in improving the state-of-the-art finite element technology (see [3]) and meshfree technology (see [2,19,24,25,31]). In a coming series of papers, we introduce and analyze a new class of methods, collectively called the reproducing kernel element method (RKEM), which are constructed by combining the virtues of finite element approximations and reproducing kernel particle approximations (RKPM, [7,21–23]). This is the first paper (Part I) of a series devoted to RKEM.

* Corresponding author. Tel.: +1-847-491-7094; fax: +1-847-491-3915.
E-mail address: w-liu@northwestern.edu (W.K. Liu).

0045-7825/$ - see front matter © 2004 Elsevier B.V. All rights reserved.
doi:10.1016/j.cma.2003.12.001

In these new methods, we patch the global partition polynomials together by associating them with compactly supported functions defined through a kernel to satisfy the required reproducing conditions. The proposed RKEM enjoys some distinguished features:

1. The smoothness of the global basis functions is solely determined by that of the kernel function, and is not limited by the smoothness of the finite elements.
2. The global basis functions of RKEM have the Kronecker delta property at the associated nodes, provided that some conditions on the support size of the kernel function are met.

In finite element methods (FEM), the smoothness of FEM shape functions is limited by the inter-element boundary continuities. For example, to solve fourth-order differential equations, one needs C^1 elements in a standard conforming method. However, as it is well-known, it is not practical to use C^1 elements for problems over two or higher dimensional domains. The proposed RKEM eliminates this difficulty and can be used as a smoothing technique to obtain consistent solution in derivative in the framework of FEM [27]. On the other hands, for most of meshfree methods, the treatment of Dirichlet boundary conditions is problematic due to the loss of the Kronecker delta property of meshfree shape functions. In the literature, a variety of techniques were proposed and analyzed for enforcing Dirichlet boundary conditions, e.g., Lagrangian multiplier technique [2], transformation technique [6], hierarchical enrichment technique [13,29], reproducing kernel interpolation technique [5], singular kernel function technique [6,17], collocation technique [30], window or correction function [10], and use of D'Alembert's principle [9]. Nevertheless, most of these techniques do not have good scalability in parallel computations.

On the contrary, for the proposed RKEM, the Kronecker delta property is kept as long as certain conditions on the support size of the kernel function are satisfied. Thus the treatment of Dirichlet boundary conditions in RKEM is straightforward. Moreover, as was noted in [12], most of the available techniques for imposing Dirichlet boundary conditions have optimal convergence rate *only when* the polynomial reproducing order is one for two or higher dimensional problems. Numerical results reported in Section 5 shows RKEM maintains optimal numerical convergence rates when it is used to solve a Dirichlet boundary value problem with any polynomial reproducing degree higher than one for multiple dimensional problems.

Similar ideas were explored in Hao et al. [16], and Hao and Liu [14,15], where the so-called moving particle finite element methods were introduced. These methods tried to achieve the following objectives: (1) no numerically induced discontinuity between elements; (2) no special treatment required for enforcing essential boundary conditions; and (3) efficiency in implementation and computation. However, numerical results based on the nodal/particle integration scheme in [14–16] shows numerical oscillations, especially for coarse finite element meshes. The framework for the development of RKEM is different from that of the moving particle finite element methods.

As the first paper in the series, the main objective is to provide a solid theoretical foundation to the method. The outline of the paper is as follows: In Section 2, the reproducing kernel element method, RKEM, is introduced as a hybrid of the traditional finite element approximation and the more recent reproducing kernel approximation technique. We show that the polynomial reproducing property of the finite element functions is maintained by the reproducing kernel element functions without additional effort. Moreover, under some provisions, the reproducing degree can be increased by including additional, minimal number of terms associated with the reproducing kernel. In Section 3, we investigate two properties of RKEM. The first is the interpolation property of the reproducing kernel element functions at the nodes. This is equivalent to the Kronecker delta property of the related global basis functions. This property is useful in imposing Dirichlet boundary conditions. The second property is the smoothness of the reproducing kernel element functions, which is shown to be solely determined by the smoothness of the kernel function. Thus, functions with a good approximation property and any degree of smoothness can be constructed with ease. In Section 4, we give a detailed error analysis of the method in the case of the linear

reproducing property. Error estimation is done through an extension of the arguments given in [11,18,23] for RKPM. Numerical examples are included in Section 5 to demonstrate the effectiveness and efficiency of the proposed method. Finally, some concluding remarks are given in Section 6.

We now introduce some notations that will be used throughout the paper. The letter d is a positive integer and is used for the spatial dimension, $d \leqslant 3$ for most applications. A generic point in $\mathbb{R}^d$ is denoted by $\boldsymbol{x} = (x_1, \ldots, x_d)^{\mathrm{T}}$, or $\boldsymbol{y} = (y_1, \ldots, y_d)^{\mathrm{T}}$ or $\boldsymbol{z} = (z_1, \ldots, z_d)^{\mathrm{T}}$. The length of a vector is measured by the Euclidean norm

$$\|\boldsymbol{x}\| = \left(\sum_{i1}^{d} |x_i|^2 \right)^{1/2},$$

or the maximum norm

$$\|\boldsymbol{x}\| = \max_{1 \leqslant i \leqslant d} |x_i|.$$

With the latter choice, a circle or a sphere is represented by an ordinary square or cube, and the support of the window function used in the method will be a square or cube. In contrast, with the choice of the Euclidean norm, the support of the window function will be an ordinary circle or sphere. Our description and analysis of the method are valid for any choice of the vector norm.

It is convenient to use the multi-index notation for partial derivatives. A multi-index is an ordered collection of d non-negative integers, $\alpha = (\alpha_1, \ldots, \alpha_d)$. The quantity $|\alpha| = \sum_{i=1}^{d} \alpha_i$ is said to be the length of α. For $\boldsymbol{z} = (z_1, \ldots, z_d)^{\mathrm{T}} \in \mathbb{R}^d$ and $\alpha = (\alpha_1, \ldots, \alpha_d)$, we write $\boldsymbol{z}^{\alpha} = z_1^{\alpha_1}, \ldots, z_d^{\alpha_d}$.

2. Reproducing kernel element interpolant

Let $\Omega \subset \mathbb{R}^d$ be an open, bounded domain with a Lipschitz continuous boundary $\Gamma = \partial\Omega$. Let there be a subdivision $\{\Omega_n\}_{n1}^{N}$ of the domain $\overline{\Omega} = \Omega \cup \Gamma$, i.e.:

1. Each Ω_n is a closed set with a non-empty interior.
2. $\overline{\Omega} = \bigcup_{n=1}^{N} \Omega_{n_\delta}$
3. For $m \neq n$, $\Omega_m \cap \overset{\circ}{\Omega}_n = \emptyset$, where $\overset{\circ}{\Omega}_m$ denotes the interior of Ω_m.

On each subdomain Ω_n, we assume that for some integer $I_n \geqslant 1$, there are linearly independent functions $\{\psi_{n,i}\}_{i=1}^{I_n}$ and corresponding nodes $\{\boldsymbol{x}_{n,i}\}_{i=1}^{I_n} \subset \Omega_n$, such that the following *reproducing property of order k* holds:

$$\sum_{i=1}^{I_n} \psi_{n,i}(\boldsymbol{x}) \boldsymbol{x}_{n,i}^{\gamma} = \boldsymbol{x}^{\gamma} \quad \forall \gamma : |\gamma| \leqslant k \ \forall \boldsymbol{x} \in \overline{\Omega}. \tag{2.1}$$

We call the basis functions, $\{\psi_{n,i}\}_{i=1}^{I_n}$, the *global partition polynomials*. They are essentially C^{∞} functions, whose properties will be further examined in the Part II [20] of this work.

As an example that will be considered in detail later in the paper, we can take the subdivision $\{\Omega_n\}_{n=1}^{N}$ as a finite element partition of the domain $\overline{\Omega}$ into triangular or tetrahedral elements, and use the associated linear elements. Then for each element Ω_n, we take $I_n = d + 1$, $\{\boldsymbol{x}_{n,i}\}_{i=1}^{d+1}$ to be the vertices, and $\{\psi_{n,i}\}_{i=1}^{d+1}$ the natural extension of the linear basis functions to the whole space $\mathbb{R}^d$. For instance, for a one-dimensional setting, with $\Omega_n = [x_{n-1}, x_n]$, we let

$$\psi_{n,1}(x) = \frac{x_n - x}{x_n - x_{n-1}}, \qquad \psi_{n,2}(x) = \frac{x - x_{n-1}}{x_n - x_{n-1}}$$

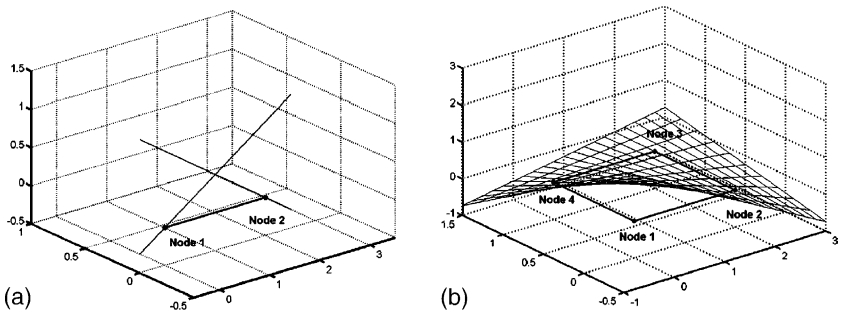

Fig. 1. Global partition polynomials in 1-D and 2-D: (a) 1-D linear global partition polynomials; and (b) 2-D bilinear global partition polynomials.

defined for any $x \in \mathbb{R}$. Linear global partition polynomials in 1-D and bilinear global partition polynomials in 2-D are plotted in Fig. 1(a) and (b), respectively.

In the new method studied in this paper, we patch the local approximation functions together by associating them with compactly supported functions defined through kernel functions of special forms. For this purpose, let us introduce a kernel function $K_\rho(\boldsymbol{z};\boldsymbol{x})$ such that it is non-zero only when $\|\boldsymbol{z}\| < \rho$. The positive number ρ represents the support size of the kernel function with respect to its first argument. Later on, we will be more specific on the form of the function $K_\rho(\boldsymbol{z};\boldsymbol{x})$. Then we define the following (quasi)interpolation operator on a continuous function $v \in C(\overline{\Omega})$:

$$\mathscr{I}v(\boldsymbol{x}) = \sum_{n=1}^{N}\left[\int_{\Omega_n} K_\rho(\boldsymbol{y}-\boldsymbol{x};\boldsymbol{x})\,\mathrm{d}\boldsymbol{y}\sum_{i=1}^{I_n}\psi_{n,i}(\boldsymbol{x})v(\boldsymbol{x}_{n,i})\right]. \tag{2.2}$$

Note that it is possible to use a different support size on a different subdomain, and this will be the topic in a forthcoming paper. Voronoi diagram can be used as a reference to model refinement and support size choice [26] in an irregular discretization. As shown in Fig. 2, the nodes involved in the evaluation of $\mathscr{I}v(\boldsymbol{x})$ at a point $\boldsymbol{x}$ depend on the support size ρ.

For the interpolation operator $\mathscr{I}$, we have the following result on its polynomial reproducing property.

Proposition 2.1. *Assume the reproducing property* (2.1) *for each subdomain. Then the interpolation operator* $\mathscr{I}$ *defined in* (2.2) *has the reproducing property of order* k:

$$\mathscr{I}\boldsymbol{x}^\gamma = \boldsymbol{x}^\gamma \quad \forall\gamma : |\gamma| \leqslant k,\ \boldsymbol{x} \in \overline{\Omega} \tag{2.3}$$

if and only if it has the reproducing property of order 0:

$$\mathscr{I}1. \tag{2.4}$$

Proof. We only need to show that (2.4) implies (2.3). Let γ be such that $|\gamma| \leqslant k$. Then using the assumption (2.1), we have

$$\mathscr{I}\boldsymbol{x}^\gamma = \sum_{n1}^{N}\left[\int_{\Omega_n} K_\rho(\boldsymbol{y}-\boldsymbol{x};\boldsymbol{x})\,\mathrm{d}\boldsymbol{y}\sum_{i1}^{I_n}\psi_{n,i}(\boldsymbol{x})\boldsymbol{x}_{n,i}^\gamma\right] = \sum_{n1}^{N}\left[\int_{\Omega_n} K_\rho(\boldsymbol{y}-\boldsymbol{x};\boldsymbol{x})\,\mathrm{d}\boldsymbol{y}\boldsymbol{x}^\gamma\right] = \boldsymbol{x}^\gamma\mathscr{I}1.$$

Since $\mathscr{I}1$, we conclude $\mathscr{I}\boldsymbol{x}^\gamma = \boldsymbol{x}^\gamma$. □

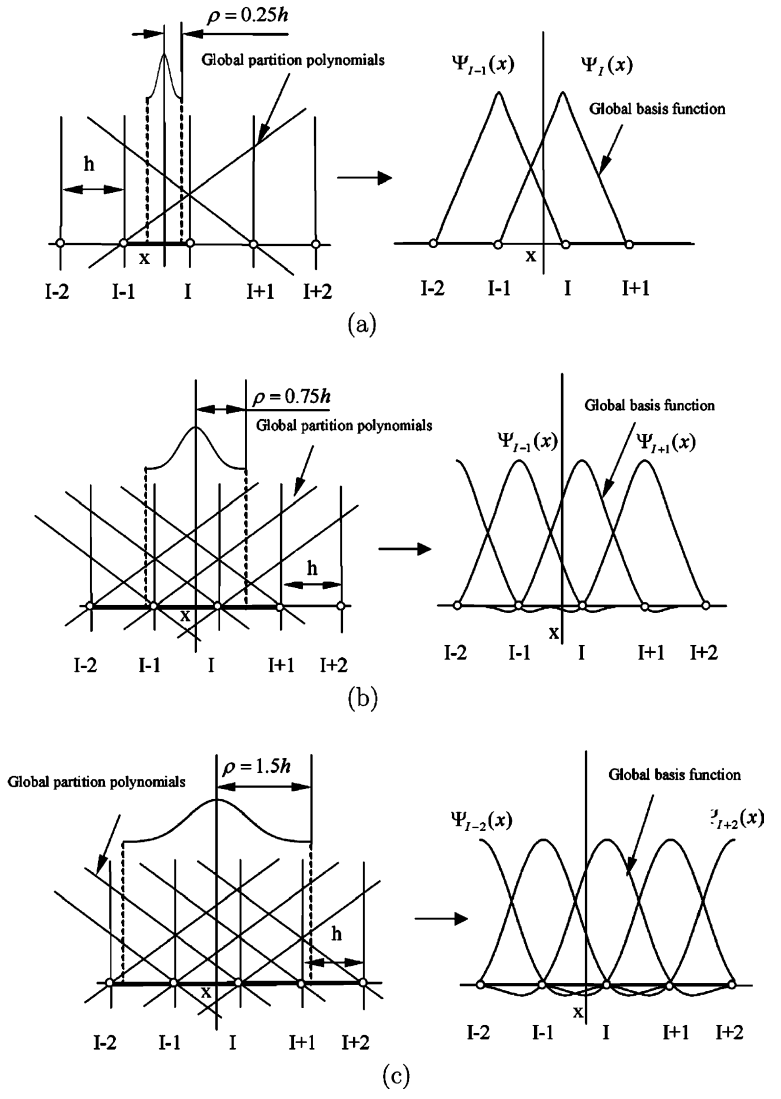

Fig. 2. A reproducing kernel element approximation with a different support size for evaluation point x: (a) $\mathscr{I}v(x) = \Psi_{I-1}(x)v_{I-1} + \Psi_I(x)v_I$, $\rho = 0.25h$, (b) $\mathscr{I}v(x) = \Psi_{I-2}(x)v_{I-2} + \Psi_{I-1}(x)v_{I-1} + \Psi_I(x)v_I + \Psi_{I+1}(x)v_{I+1}$, $\rho = 0.75h$, and (c) $\mathscr{I}v(x) = \Psi_{I-2}(x)v_{I-2} + \Psi_{I-1}(x)v_{I-1} + \Psi_I(x)v_I + \Psi_{I+1}(x)v_{I+1} + \Psi_{I+2}(x)v_{I+2}$, $\rho = 1.5h$.

The condition (2.4) can be more conveniently restated as

$$\int_\Omega K_\rho(\boldsymbol{y} - \boldsymbol{x}; \boldsymbol{x})\,\mathrm{d}\boldsymbol{y} = 1 \quad \forall \boldsymbol{x} \in \overline{\Omega}. \tag{2.5}$$

For some integer $m \geqslant k$, we require the interpolation operator $\mathscr{I}$ defined in (2.2) to have a reproducing property of order m. By Proposition 2.1, this is equivalent to the conditions

$$\mathscr{I}\boldsymbol{x}^\alpha = \boldsymbol{x}^\alpha \quad \forall \alpha : |\alpha| 0, k+1, \ldots, m \ \forall \boldsymbol{x} \in \Omega. \tag{2.6}$$

From now on, we will focus on the following particular choice for the kernel function

$$K_\rho(\boldsymbol{z};\boldsymbol{x}) = \frac{1}{\rho^d}\phi\left(\frac{\boldsymbol{z}}{\rho}\right)\boldsymbol{p}\left(\frac{\boldsymbol{z}}{\rho}\right)^{\mathrm{T}}\boldsymbol{b}(\boldsymbol{x}), \tag{2.7}$$

where

$$\boldsymbol{p}(\boldsymbol{z}) = (1, z_1^{k+1}, z_1^k z_2, \ldots, z_d^{k+1}, z_1^{k+2}, \ldots, z_d^m)^{\mathrm{T}}$$

is the vector of constant 1 and the monomials of degree between $(k+1)$ and m: $\boldsymbol{z}^\alpha$ for $|\alpha| = k+1, \ldots, m$. The variable vector $\boldsymbol{b}$ has the same dimension as the vector $\boldsymbol{p}$. The function ϕ is the *window function*, and has a support size 1. The interpolant of a continuous function $v \in C(\overline{\Omega})$ can then be written as

$$\mathscr{I}v(\boldsymbol{x}) = \sum_{n1}^{N}\left[\int_{\Omega_n}\frac{1}{\rho^d}\phi\left(\frac{\boldsymbol{y}-\boldsymbol{x}}{\rho}\right)\boldsymbol{p}\left(\frac{\boldsymbol{y}-\boldsymbol{x}}{\rho}\right)^{\mathrm{T}}\boldsymbol{b}(\boldsymbol{x})\,\mathrm{d}\boldsymbol{y}\sum_{i1}^{I_n}\psi_{n,i}(\boldsymbol{x})v(\boldsymbol{x}_{n,i})\right]. \tag{2.8}$$

Use this form of the kernel function, the conditions (2.6) can be rewritten as a linear system for the unknown variable coefficient vector $\boldsymbol{b}(\boldsymbol{x})$:

$$\sum_{n1}^{N}\left[\int_{\Omega_n}\frac{1}{\rho^d}\phi\left(\frac{\boldsymbol{y}-\boldsymbol{x}}{\rho}\right)\boldsymbol{p}\left(\frac{\boldsymbol{y}-\boldsymbol{x}}{\rho}\right)^{\mathrm{T}}\mathrm{d}\boldsymbol{y}\sum_{i1}^{I_n}\psi_{n,i}(\boldsymbol{x})\boldsymbol{x}_{n,i}^{\alpha}\right]\boldsymbol{b}(\boldsymbol{x}) = \boldsymbol{x}^\alpha \quad \forall\alpha : |\alpha|0, k+1, \ldots, m. \tag{2.9}$$

Equivalently, the system can be rewritten as

$$\sum_{n=1}^{N}\left[\int_{\Omega_n}\frac{1}{\rho^d}\phi\left(\frac{\boldsymbol{y}-\boldsymbol{x}}{\rho}\right)\boldsymbol{p}\left(\frac{\boldsymbol{y}-\boldsymbol{x}}{\rho}\right)^{\mathrm{T}}\mathrm{d}\boldsymbol{y}\sum_{i=1}^{I_n}\psi_{n,i}(\boldsymbol{x})\left(\frac{\boldsymbol{x}-\boldsymbol{x}_{n,i}}{\rho}\right)^{\alpha}\right]\boldsymbol{b}(\boldsymbol{x}) = \delta_{|\alpha|,0} \quad \forall\alpha : |\alpha| = 0, k+1, \ldots, m. \tag{2.10}$$

The discussion on solvability of a higher order RKEM system will be deferred in a sequel paper.

In this paper, we first illustrate, in detail, the procedure to construct the global RKEM shape function with the first-order polynomial reproducing capacity. Consider a 1-D example of RKEM interpolant with the first-order reproducing condition and linear global partition polynomials. Since the basis function satisfies linear consistency, by Proposition 2.1, we need only to reproduce a constant to satisfy the first-order reproducing conditions. In this case, $\boldsymbol{p}(z) = 1$ and $\boldsymbol{b}(x) = b_0(x)$. By (2.7), the kernel function is

$$K_\rho(\boldsymbol{y}-\boldsymbol{x};\boldsymbol{x}) = b_0(x)\frac{1}{\rho}\phi\left(\frac{\boldsymbol{y}-\boldsymbol{x}}{\rho}\right), \tag{2.11}$$

while the interpolation function (2.2) becomes

$$\mathscr{I}v(x) = \sum_{n=1}^{N}\left[\int_{\Omega_n} b_0(x)\frac{1}{\rho}\phi\left(\frac{\boldsymbol{y}-\boldsymbol{x}}{\rho}\right)\mathrm{d}\boldsymbol{y}\sum_{i=1}^{I_n}\psi_{n,i}(x)v(x_{n,i})\right]. \tag{2.12}$$

The coefficient function $b_0(x)$ is determined by the zeroth consistency condition

$$1 = \sum_{n=1}^{N}\int_{\Omega_n} b_0(x)\frac{1}{\rho}\phi\left(\frac{\boldsymbol{y}-\boldsymbol{x}}{\rho}\right)\mathrm{d}\boldsymbol{y},$$

and we have

$$b_0(x) = \left[\int_{\Omega}\frac{1}{\rho}\phi\left(\frac{\boldsymbol{y}-\boldsymbol{x}}{\rho}\right)\mathrm{d}\boldsymbol{y}\right]^{-1}. \tag{2.13}$$

The proposed approximation can be explicitly expressed as

$$\mathscr{I}v(x) = \sum_{n=1}^{N} b_0(x)\left[\int_{\Omega_n}\frac{1}{\rho}\phi\left(\frac{\boldsymbol{y}-\boldsymbol{x}}{\rho}\right)\mathrm{d}\boldsymbol{y}\sum_{i=1}^{I_n}\varphi_{n,i}(x)v(x_{n,i})\right] = \sum_{I}\Psi_I(x)v_I. \tag{2.14}$$

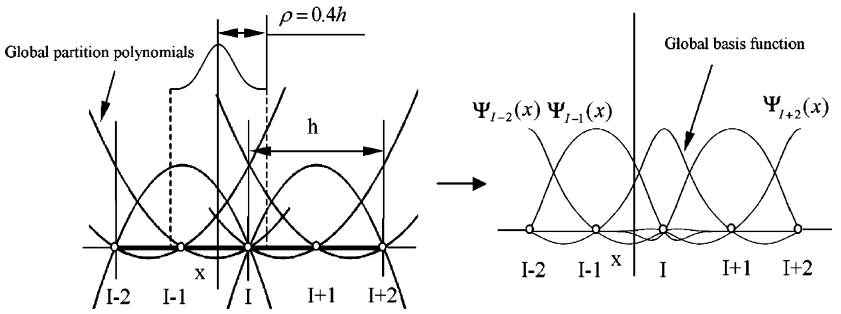

Fig. 3. A reproducing kernel element interpolation with a quadratic basis function for evaluation point x: $\mathscr{I}v(x) = \Psi_{I-2}(x)v_{I-2} + \Psi_{I-1}(x)v_{I-1} + \Psi_I(x)v_I + \Psi_{I+1}(x)v_{I+1} + \Psi_{I+2}(x)v_{I+2}$ with quadratic basis function.

Reproducing kernel element approximation for evaluation point x in a 1-D uniform partition with different support sizes and a linear basis function are constructed as shown in Fig. 2, and a reproducing kernel element interpolation for evaluation point x in a 1-D uniform partition with quadratic basis function is constructed as shown in Fig. 3.

3. Some properties

In this section, we assume the system (2.9) or (2.10) is uniquely solvable at any $\boldsymbol{x} \in \overline{\Omega}$. This assumption for the general case, together with rigorous error analysis of the method, will be given in detail in another paper. For various particular cases, such as the one with $m = k1$ to be considered in Section 4, the unique solvability of the linear system is straightforward.

We now examine two properties of the reproducing kernel element method introduced in Section 2. The first is the Kronecker delta property of the global basis functions associated with the interpolation operator $\mathscr{I}$. We will denote the collection of the nodes of the method by $\{\boldsymbol{x}_j\}_{j1}^{J}$. For each $j1, \ldots, J$, the node $\boldsymbol{x}_j$ equals $\boldsymbol{x}_{n,i}$ for some n and some i, $1 \leqslant i \leqslant I_n$, $1 \leqslant n \leqslant N$. Some of the nodes $\boldsymbol{x}_j$ belong to more than one subdomain (element). For the node $\boldsymbol{x}_j$, we denote $B(\boldsymbol{x}_j; \rho)$ the ball of radius ρ centered at $\boldsymbol{x}_j$, and denote $\Omega(\boldsymbol{x}_j)$ the union of the subdomains that contain $\boldsymbol{x}_j$ as a node.

Proposition 3.1. *Assume the basis function* $\{\psi_{n,i}\}_{i1}^{I_n}$ *are nodal basis functions, i.e., they satisfy*

$$\psi_{n,i}(\boldsymbol{x}_{n,j}) = \delta_{i,j}, \quad 1 \leqslant i, j \leqslant I_n. \tag{3.1}$$

Also assume

$$B(\boldsymbol{x}_j; \rho) \subset \Omega(\boldsymbol{x}_j), \quad 1 \leqslant j \leqslant J. \tag{3.2}$$

Then the interpolation operator $\mathscr{I}$ *defined in* (2.2) *enjoys the interpolation condition: for any continuous function* $v \in C(\overline{\Omega})$,

$$\mathscr{I}v(\boldsymbol{x}_j) = v(\boldsymbol{x}_j), \quad 1 \leqslant j \leqslant J. \tag{3.3}$$

Proof. We have

$$\mathscr{I}v(\boldsymbol{x}_j) = \sum_{n1}^{N} \left[\int_{\Omega_n} K_\rho(\boldsymbol{y} - \boldsymbol{x}_j; \boldsymbol{x}_j)\, \mathrm{d}\boldsymbol{y} \sum_{i1}^{I_n} \psi_{n,i}(\boldsymbol{x}_j) v(\boldsymbol{x}_{n,i}) \right].$$

Note that $K_\rho(\boldsymbol{y}-\boldsymbol{x}_j;\boldsymbol{x}_j)$ is non-zero only if $\|\boldsymbol{y}-\boldsymbol{x}_j\| \leqslant \rho$. Using the assumptions (3.2) and (3.1), we find

$$\mathscr{I}v(\boldsymbol{x}_j) = \int_{\Omega(\boldsymbol{x}_j)} K_\rho(\boldsymbol{y}-\boldsymbol{x}_j;\boldsymbol{x}_j)v(\boldsymbol{x}_j)\,\mathrm{d}\boldsymbol{y} = v(\boldsymbol{x}_j)\int_\Omega K_\rho(\boldsymbol{y}-\boldsymbol{x}_j;\boldsymbol{x}_j)\,\mathrm{d}\boldsymbol{y}.$$

By the zeroth order reproducing property (2.5), we then obtain the interpolation property (3.3). □

The condition (3.2) imposes a restriction on the size of ρ: it has to be small enough. In the case of linear elements and only vertices of the elements are used as the nodes, then ρ must be smaller than a constant times $\min_{1\leqslant n\leqslant N} h_n$. The constant depends on the shape regularity of the finite element partition. If side mid-points are used as the nodes (quadratic elements), then ρ should be smaller than the constant times $0.5\min_{1\leqslant n\leqslant N} h_n$. Now if we like to have the Kronecker delta property only for the global basis functions associated with the nodes on the Dirichlet boundary, then $\min_{1\leqslant n\leqslant N} h_n$ can be replaced by $\min_{1\leqslant n\leqslant N_0} h_n$, where $\Omega_1,\ldots,\Omega_{N_0}$ denote the elements on the boundary that contain Dirichlet boundary nodes. To be specific, in the 1-D case with a uniform partition and linear reproducing, the condition is $\rho \leqslant h$.

The second property is on the differentiability of the interpolation function $\mathscr{I}v$, i.e., the differentiability of the global basis function associated with the interpolation operator $\mathscr{I}$.

Proposition 3.2. *Assume the basis functions $\psi_{n,i} \in C^{k_1}(\overline{\Omega})$, $1\leqslant i\leqslant I_n$, $1\leqslant n\leqslant N$. Assume the window function $\phi \in C^{k_2}(\mathbb{R}^d)$. Here, k_1 and k_2 are two non-negative integers. Then for any continuous function $v\in C(\overline{\Omega})$, its interpolant $\mathscr{I}v \in C^{\min(k_1,k_2)}(\overline{\Omega})$.*

Proof. From (2.10), we see that each component of $\boldsymbol{b}$ is a $C^{\min(k_1,k_2)}(\overline{\Omega})$ function. The result of the proposition follows immediately from the representation formula (2.8). □

We notice that in the context of triangular finite elements, the basis functions $\psi_{n,i}$ are polynomials, and are thus infinitely smooth. Then the regularity of the global basis functions of the new method is the same as that of the window function ϕ.

A set of global basis functions and its derivative for 1-D case with support size $\rho 0.95h$, and the linear basis function and cubic B-spline kernel are plotted in Fig. 4(a) and (b), respectively. The Kronecker delta property and continuity of the global basis functions are clearly illustrated.

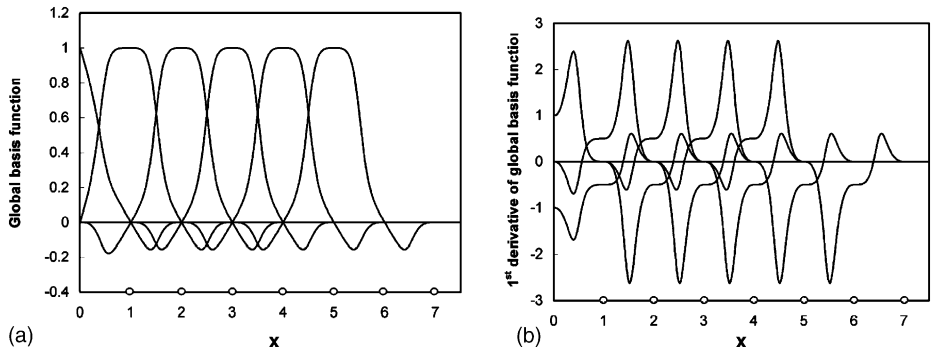

Fig. 4. A set of global basis functions and their derivative in 1-D domain: (a) RKEM global basis function; and (b) the 1st derivative of RKEM global basis function.

Note that based on the definition, the RKE interpolation formula (2.2) is involved with an integral. There are several ways to evaluate this integral to obtain the explicit expression for a RKE shape function, $\Psi_I(x)$, see Eq. (2.14). The RKE shape functions and their derivatives shown in Fig. 4(a) and (b) are constructed based on a nodal integration scheme proposed in Part II of this series (see [20]). The advantage of using nodal integration to evaluate the integral is that it can provide an explicit expression of RKE interpolant. Nonetheless, the RKE shape functions used in the numerical examples of this paper are all constructed by evaluating the integral via Gauss quadrature.

4. Error analysis of the method with linear reproducing property

In this section, we give a detailed analysis of the method with $m = k1$ and when linear finite elements are used for the local approximations. To simplify the exposition, we let $d \leqslant 3$. The method for more general cases is being analyzed. Throughout the section, c denotes a generic constant that does not depend on the discretization parameters and functions under consideration. We first list various assumptions.

We assume that $\{\{\Omega_n\}_{n1}^N\}$ is a family of quasiuniform finite element partition of the domain $\overline{\Omega}$ into triangular or tetrahedral elements. For a mesh $\{\Omega_n\}_{n1}^N$ in the family, we let h be the mesh size, and let h_n be the diameter of Ω_n. Since the mesh family is quasiuniform, we have a constant $c > 0$ such that

$$ch \leqslant h_n \leqslant h, \quad 1 \leqslant n \leqslant N. \tag{4.1}$$

Associated with each mesh $\{\Omega_n\}_{n1}^N$, we define a parameter ρ, intended for the support size of the reproducing kernel function. We assume that there exists a constant $c \geqslant 1$ such that

$$c^{-1}h \leqslant \rho \leqslant ch. \tag{4.2}$$

For the window function ϕ, we assume

$$\begin{cases} \text{supp}(\phi)B_1, \\ \phi(\boldsymbol{x}) > 0 \quad \text{for } \|\boldsymbol{x}\| < 1, \\ \phi \in C^l(\mathbb{R}^d) \quad \text{for some } l \geqslant 1. \end{cases} \tag{4.3}$$

Here, $B_1 = \{\boldsymbol{x} \in \mathbb{R}^d \,|\, \|\boldsymbol{x}\| \leqslant 1\}$ is the unit ball.

For a continuous function $v \in C(\overline{\Omega})$, the interpolant is (cf. (2.8))

$$\mathscr{I}_1 v(\boldsymbol{x}) = \sum_{n1}^{N} \left[\int_{\Omega_n} \frac{1}{\rho^d} \phi\left(\frac{\boldsymbol{y}-\boldsymbol{x}}{\rho}\right) \mathrm{d}\boldsymbol{y} \sum_{i1}^{d+1} \psi_{n,i}(\boldsymbol{x}) v(\boldsymbol{x}_{n,i}) \right] b_0(\boldsymbol{x}), \tag{4.4}$$

where the coefficient function $b_0(\boldsymbol{x})$ is determined by the zeroth reproducing condition

$$b_0(\boldsymbol{x}) = \left[\int_{\Omega} \frac{1}{\rho^d} \phi\left(\frac{\boldsymbol{y}-\boldsymbol{x}}{\rho}\right) \mathrm{d}\boldsymbol{y} \right]^{-1}. \tag{4.5}$$

Note that by Proposition 2.1, we have

$$\mathscr{I}_1 v(\boldsymbol{x}) = v(\boldsymbol{x})$$

for any linear function v.

From the formula (4.5) and assumptions (4.3), (4.2), it is readily verified that

$$\max_{\boldsymbol{x} \in \overline{\Omega}} |b_0(\boldsymbol{x})| + h \max_{\boldsymbol{x} \in \overline{\Omega}} \max_{1 \leqslant i \leqslant d} |\partial_i b_0(\boldsymbol{x})| \leqslant c. \tag{4.6}$$

Now let $u \in H^2(\Omega)$ and let us bound the interpolation error $u - \mathscr{I}_1 u$. By the Sobolev embedding theorem, we have $u \in C(\overline{\Omega})$ and so $\mathscr{I}_1 u$ is well defined. We first bound the interpolation error on a typical element Ω_j. Define

$$\widetilde{\Omega}_j = \{\boldsymbol{x} \in \overline{\Omega} | \mathrm{dist}(\boldsymbol{x}, \Omega_j) \leqslant \rho\}.$$

We denote $\psi_{j,i}(\boldsymbol{x})$, $1 \leqslant i \leqslant d+1$, the natural extensions of the linear element shape functions corresponding to the $d+1$ vertices of the element Ω_j. Note that $\{\psi_{j,i}(\boldsymbol{x})\}_{i1}^{d+1}$ are linear functions defined on the whole space $\mathbb{R}^{\mathbb{d}}$. Using (4.1), we find that

$$\max_{1 \leqslant i \leqslant d+1} \|\psi_{j,i}\|_{C(\tilde{\Omega}_j)} + h \max_{1 \leqslant i \leqslant d+1} \|\psi_{j,i}\|_{C^1(\tilde{\Omega}_j)} \leqslant c. \tag{4.7}$$

Introduce the linear interpolation function

$$\mathscr{I}_{1,j} u(\boldsymbol{x}) = \sum_{i1}^{d+1} \psi_{j,i}(\boldsymbol{x}) u(\boldsymbol{x}_{j,i}).$$

By a standard scaling argument (cf. [4,8]), we have the error estimate

$$\|u - \mathscr{I}_{1,j} u\|_{L^2(\tilde{\Omega}_j)} + h\|u - \mathscr{I}_{1,j} u\|_{H^1(\tilde{\Omega}_j)} + h^{d/2}\|u - \mathscr{I}_{1,j} u\|_{L^\infty(\tilde{\Omega}_j)} \leqslant ch^2 |u|_{H^2(\tilde{\Omega}_j)}. \tag{4.8}$$

Since $\mathscr{I}_1$ reproduces linear functions, we have

$$\mathscr{I}_1(\mathscr{I}_{1,j} u) = \mathscr{I}_{1,j} u.$$

Write

$$u - \mathscr{I}_1 u = u - \mathscr{I}_{1,j} u - \mathscr{I}_1(u - \mathscr{I}_{1,j} u). \tag{4.9}$$

By the definition (4.4),

$$\mathscr{I}_1(u - \mathscr{I}_{1,j} u)(\boldsymbol{x}) = \sum_{n1}^{N} \left[\int_{\Omega_n} \frac{1}{\rho^d} \phi\left(\frac{\boldsymbol{y} - \boldsymbol{x}}{\rho}\right) \mathrm{d}\boldsymbol{y} \sum_{i1}^{d+1} \psi_{n,i}(\boldsymbol{x})(u - \mathscr{I}_{1,j} u)(\boldsymbol{x}_{n,i}) \right] b_0(\boldsymbol{x}).$$

Note that for $\boldsymbol{x} \in \Omega_j$, the term with the index n in the summation is possibly non-zero only if $\Omega_n \cap \widetilde{\Omega}_j \neq \emptyset$. Using the bounds (4.6) and (4.7), we then have

$$\|\mathscr{I}_1(u - \mathscr{I}_{1,j} u)\|_{H^1(\Omega_j)} \leqslant ch^{-1}\|u - \mathscr{I}_{1,j} u\|_{L^\infty(\tilde{\Omega}_j)} |\widetilde{\Omega}_j|^{1/2}.$$

Here, $|\widetilde{\Omega}_j|$ denotes the volume of the region $\widetilde{\Omega}_j$, $|\widetilde{\Omega}_j| \leqslant ch^d$. Applying the estimate (4.8), we obtain

$$\|\mathscr{I}_1(u - \mathscr{I}_{1,j} u)\|_{H^1(\Omega_j)} \leqslant ch|u|_{H^2(\tilde{\Omega}_j)}. \tag{4.10}$$

A similar argument show that

$$\|\mathscr{I}_1(u - \mathscr{I}_{1,j} u)\|_{L^2(\Omega_j)} \leqslant ch^2|u|_{H^2(\tilde{\Omega}_j)}. \tag{4.11}$$

From the decomposition (4.9), the error estimates (4.8), (4.10) and (4.11), we obtain

$$\|u - \mathscr{I}_1 u\|_{L^2(\Omega_j)} + h\|u - \mathscr{I}_1 u\|_{H^1(\Omega_j)} \leqslant ch^2|u|_{H^2(\tilde{\Omega}_j)}, \quad 1 \leqslant j \leqslant N.$$

Then we have the following global interpolation error estimates:

$$\|u - \mathscr{I}_1 u\|_{L^2(\Omega)} + h\|u - \mathscr{I}_1 u\|_{H^1(\Omega)} \leqslant ch^2|u|_{H^2(\Omega)}. \tag{4.12}$$

Theorem 4.1. *Consider a spatial discretization satisfying the assumptions* (4.1) *and* (4.2). *Construct the RKEM interpolant with a window function satisfying condition* (4.3). *Then for any* $u \in C^0(\Omega) \cap H^2(\Omega)$, *the interpolation error estimate* (4.12) *holds*.

Consider solving a linear second-order elliptic boundary value problem. The weak formulation is:

$$\text{Find } u \in V, \quad \text{such that } a(u,v) = \ell(v) \quad \forall v \in V, \tag{4.13}$$

where $V \subset H^1(\Omega)$. The bilinear form $a(\cdot,\cdot)$ is continuous and V-elliptic, and the linear form ℓ is continuous on V. In the setting described at the beginning of the section, we define X_h to be the space of functions of the form

$$\sum_{n1}^{N}\left[\int_{\Omega_n}\frac{1}{\rho^d}\phi\left(\frac{\boldsymbol{y}-\boldsymbol{x}}{\rho}\right)\mathrm{d}\boldsymbol{y}\sum_{i1}^{d+1}\psi_{n,i}(\boldsymbol{x})\xi_{n,i}\right]b_0(\boldsymbol{x}),$$

where the coefficient function $b_0(\boldsymbol{x})$ is given in (4.5), $\xi_{n,i} \in \mathbb{R}$, and if $\boldsymbol{x}_{n_1,i_1} = \boldsymbol{x}_{n_2,i_2}$ is a node common to two elements, then $\xi_{n_1,i_1} = \xi_{n_2,i_2}$. Then we let $V_h = V \cap X_h$ and approximate the continuous problem (4.13) by

$$\text{Find } u_h \in V_h, \quad \text{such that } a(u_h,v_h) = \ell(v_h) \quad \forall v_h \in V_h. \tag{4.14}$$

By the Lax–Milgram theorem (see [4]), both (4.13) and (4.14) have unique solutions. To estimate error, we can use Céa's inequality,

$$\|u-u_h\|_{H^1(\Omega)} \leqslant c \inf_{v_h \in V_h}\|u-v_h\|_{H^1(\Omega)}.$$

Suppose the boundary condition is of Neumann or Robin type, or of Dirichlet type in the one-dimensional case. Then we can replace the term

$$\inf_{v_h \in V_h}\|u-v_h\|_{H^1(\Omega)}$$

by $\|u-\mathscr{I}_1 u\|_{H^1(\Omega)}$ in Céa's inequality, and conclude that

$$\|u-u_h\|_{H^1(\Omega)} \leqslant c\|u-\mathscr{I}_1 u\|_{H^1(\Omega)} \leqslant ch|u|_{H^2(\Omega)}$$

if the exact solution $u \in H^2(\Omega)$. Furthermore, the standard duality argument can be employed to show that

$$\|u-u_h\|_{L^2(\Omega)} \leqslant ch^2|u|_{H^2(\Omega)}.$$

In a sequel paper, we will extend the error analysis above to the more general cases. Loosely speaking, under similar assumptions on the finite element partitions and kernel functions, if the reproducing degree is m and the regularity index l in (4.3) is not smaller than m, then for the reproducing interpolant defined in (2.8), we have the error estimates

$$\|v-\mathscr{I}v\|_{H^j(\Omega)} \leqslant ch^{m+1-j}\|v\|_{H^{m+1}(\Omega)}, \quad j = 0,1,\ldots,m \ \forall v \in H^{m+1}(\Omega).$$

5. Numerical examples

In this section, we report numerical results for the performance of the proposed RKEM in solving various boundary value problems of the differential equations with special features.

5.1. A problem with rough solution

To validate the method, a special 1-D benchmark problem is solved first by using the proposed method. This problem was originally proposed by Rachford and Wheeler [28] to test the convergence property of the H^1-Galerkin method, and was used again by Babuška et al. [1] to test the mixed-hybrid finite element method, and by Liu et al. [23] to test the meshfree reproducing kernel particle method. The boundary value problem is

$$-u'' + u = f(x), \quad x \in (0,1), \tag{5.1}$$

$$u'(0) = \alpha/(1+\alpha^2\bar{x}^2), \tag{5.2}$$

$$u'(1) = -[\arctan(\alpha(1-\bar{x})) + \arctan(\alpha\bar{x})]. \tag{5.3}$$

The right side function in (5.1) is chosen as

$$f(x) = \frac{2\alpha[1+\alpha^2(1-\bar{x})(x-\bar{x})]}{[1+\alpha^2(x-\bar{x})^2]^2} + (1-x)[\arctan(\alpha(x-\bar{x})) + \arctan(\alpha\bar{x})]$$

so that the exact solution of this problem is

$$u(x) = (1-x)[\arctan(\alpha(x-\bar{x})) + \arctan(\alpha\bar{x})].$$

The solution changes its roughness as the parameter α varies. It becomes smoother as the parameter α gets smaller, and the graph of the solution has a sharp knee at location $x = \bar{x}$ when α is very large. For the numerical example here, α and $\bar{x}$ are chosen as 50.0 and 0.40, respectively. The comparison of an exact solution and numerical solution with 80 nodes is plotted in Fig. 5.

Convergence rates of the numerical solutions are first examined for global RKEM interpolants satisfying a linear consistency condition. A cubic B-spline kernel function is used to construct the reproducing kernel function. Different spatial discretizations, in which the number of nodes uniformly varies from 11 to 2561, are analyzed. Convergence rates in terms of L_2 and H^1 interpolation error norm for different support sizes are plotted in Fig. 6(a) and (b), respectively. Although the interpolation solutions are more accurate for normalized support size from 0.8 to 1.5 than that of FEM, the convergence rates are 2 and 1 in L_2 and H^1 interpolation error norm respectively. When the optimal support size $1.99h$ is chosen, convergence rate 2 in both L_2 and H^1 interpolation error norm is observed for this problem.

The same spatial discretizations are used to test the convergence rates of the proposed method. As shown in Fig. 7(a), for this example the numerical solution in the L_2 error norm is improved compared with the FEM

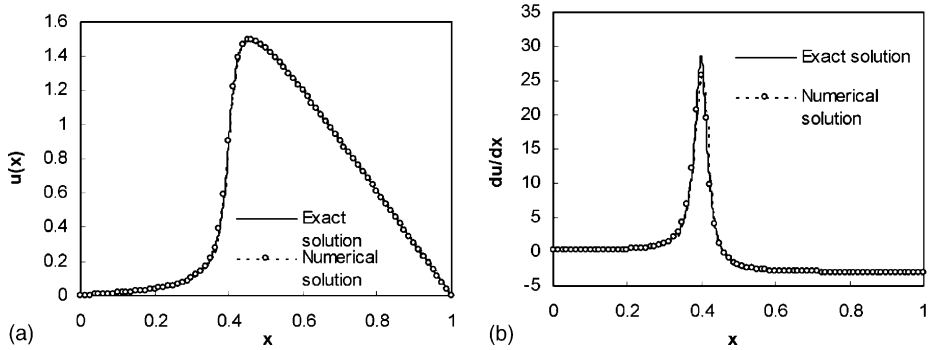

Fig. 5. Comparison between exact and numerical solutions of the benchmark problem: (a) the exact and numerical solution; and (b) the derivative of exact and numerical solution.

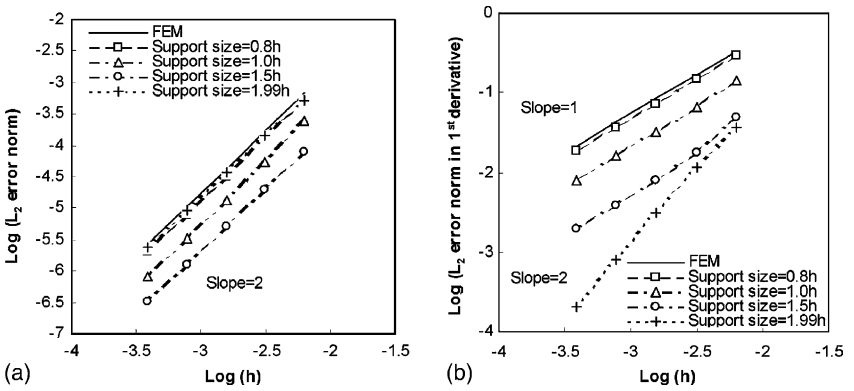

Fig. 6. Convergence rates of interpolation with different support sizes: (a) convergence rate in L_2 error norm; and (b) convergence rate in L_2 error norm with first derivative.

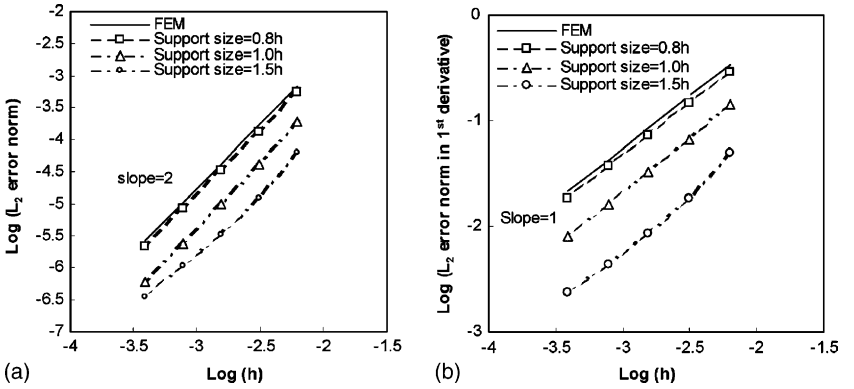

Fig. 7. Convergence rates of Galerkin solutions with different support sizes: (a) convergence rate measured in L_2 error norm; and (b) convergence rate measured in L_2 error norm with the first derivative.

solution even though they have roughly the same convergence rate index 2. The improvement in the H^1 error norm is more dramatic due to the high order continuity of global basis functions as illustrated in Fig. 7(b).

5.2. An example of a fourth-order differential equation

We consider a boundary value problem of a one-dimensional fourth-order partial differential equation in this example. For conforming approximations, we need C^1 shape functions. It is difficult to construct a C^1 shape function for FEM in two or higher dimension domain. However, shape functions with any smoothness degree can be easily constructed in any dimension for RKEM. To show the performance of RKEM on solving fourth-order problems, we apply it to the following problem:

$$u^{(4)} + u = f \quad \text{in } (0,1), \tag{5.4}$$

$$u^{(2)}(0) = u^{(3)}(0) = 1, \tag{5.5}$$

$$u^{(2)}(1) = u^{(3)}(1) = e, \tag{5.6}$$

where $f(x)2e^x$. The exact solution of this problem is $u(x) = e^x$.

Quadratic element is used to construct the basis function. Several uniform discretizations with quadratic elements are chosen in convergence study. The L_2 norms of the error in the Galerkin solution, its first and second derivatives are plotted in Figs. (8a), (9a) and (10a), respectively. The corresponding interpolation L_2 error norms in primary variable and its first and second derivatives are given in Figs. 8(b), 9(b) and 10(b). The theoretical convergence orders for the RKEM interpolation errors in L_2, H^1 and H^2 are 3, 2, and 1. For RKEM solutions, the convergence rate in H^2 norm is 1. The convergence rate of numerical solutions match the theoretical results.

5.3. A two-dimensional Dirichlet boundary value problem

The purpose of this example is to show that for Dirichlet boundary value problems, the proposed RKEM (i) can be applied directly; and (ii) maintains the optimal convergence order for any problem dimension and reproducing degree. We solve the following two-dimensional example by RKEM:

$$-\Delta u + u = f \quad \text{in } \Omega, \tag{5.7}$$

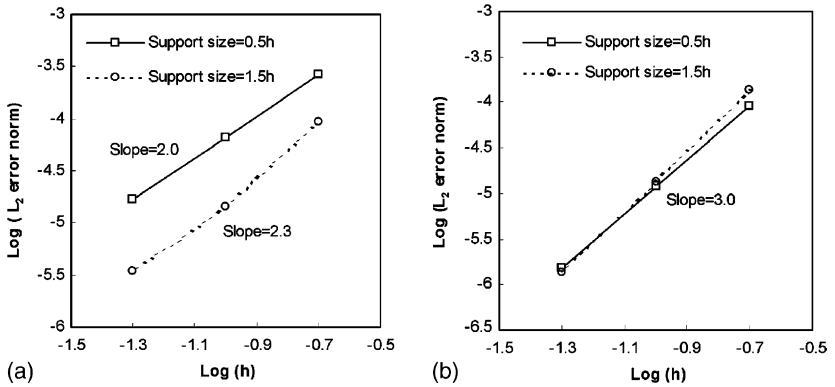

Fig. 8. L_2 norm errors for Galerkin solution and interpolation: (a) L_2 norm errors for Galerkin solution; and (b) L_2 norm errors for interpolation.

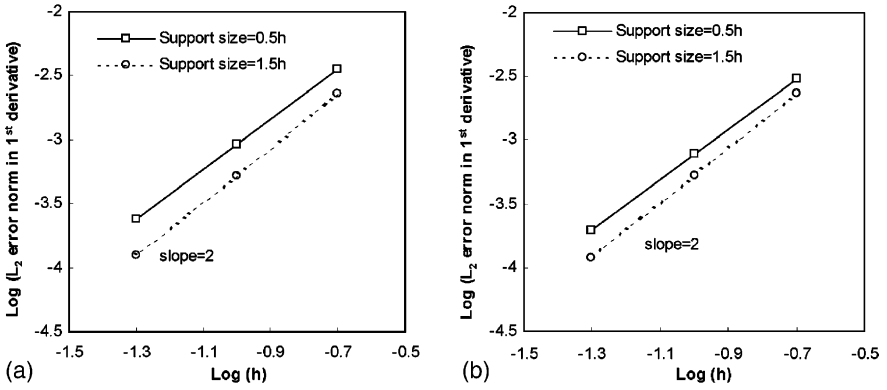

Fig. 9. L_2 norm errors for the 1st derivative of Galerkin solutions and interpolations: (a) L_2 norm errors for the 1st derivative of Galerkin solutions; and (b) L_2 norm errors for the 1st derivative of interpolations.

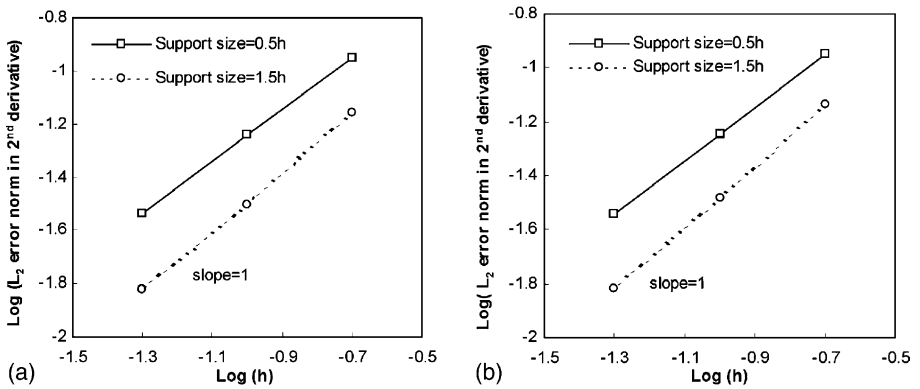

Fig. 10. L_2 norm errors for the 2nd derivative of a Galerkin solution and interpolation: (a) L_2 norm errors for the 2nd derivative of Galerkin solution; and (b) L_2 norm errors for the 2nd derivative of interpolation.

$$u = g \quad \text{on } \partial\Omega, \tag{5.8}$$

where $\Omega = (0,1)^2$, $f(x,y) = (1-x^2-y^2)e^{xy}$, and $g(x,y) = e^{xy}$.

The exact solution of this problem is $u(x,y) = e^{xy}$. A set of three spatial discretizations consisting 4×4, 8×8 and 16×16 quadratic rectangular/square elements is used in convergence study. Denote h the side of the corresponding square element. We consider two cases depending on the support size of the kernel function.

Case 1. When the support size is less than $0.5h$, the RKEM interpolant enjoys the Kronecker delta property. The numerical solution of the new method is compared with that of FEM. As shown in Figs. 11(a) and 12(a), almost the same convergence rate is observed for both methods. Unlike meshfree interpolant with quadratic basis, the convergence rate of RKEM solution in H^1 error norm is around 2.

Case 2. When the support size is larger than $0.5h$, RKEM interpolant losses the Kronecker delta property. To enforce the boundary conditions, a similar technique used in meshfree methods is adopted. As shown in Figs. 11(a) and 12(a), the accuracy of the numerical solution via RKEM in this case is actually improved compared with that of FEM.

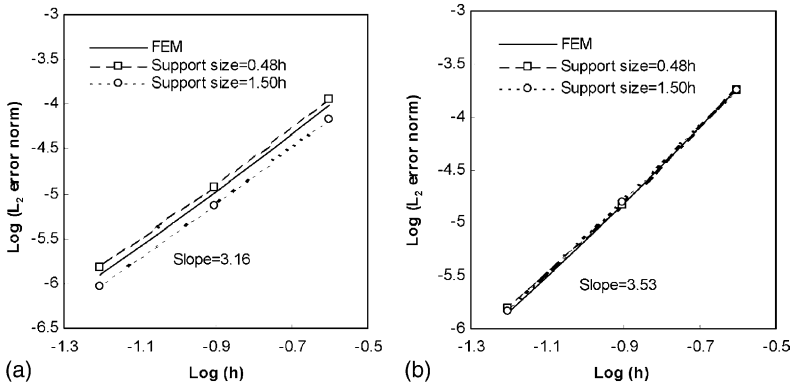

Fig. 11. L_2 norm errors for Galerkin solutions and interpolations: (a) L_2 norm errors for Galerkin solutions; and (b) L_2 norm errors for interpolations.

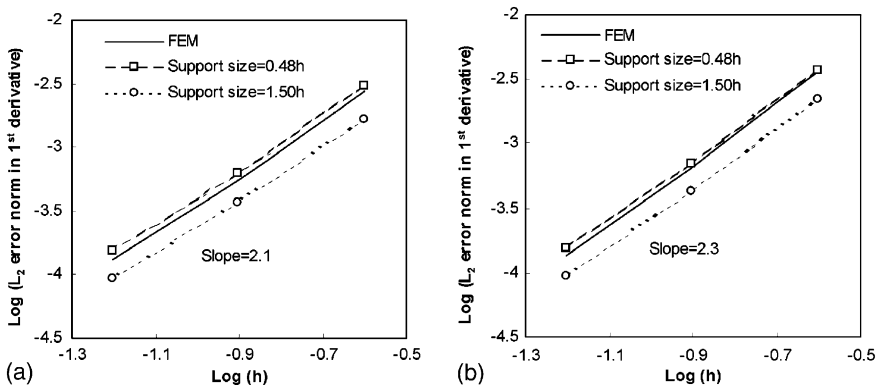

Fig. 12. L_2 norm errors for the 1st derivative of Galerkin solutions and interpolations: (a) L_2 norm errors for the 1st derivative of Galerkin solutions; and (b) L_2 norm errors for the 1st derivative of interpolations.

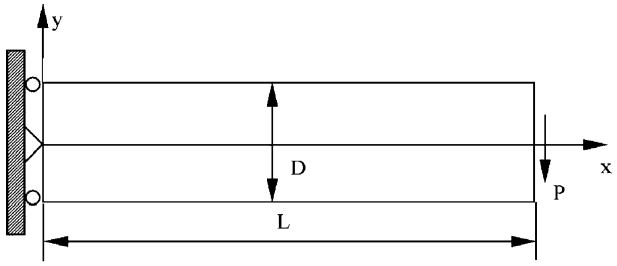

Fig. 13. Problem statement of a cantilever beam.

The comparison of interpolation results in L_2 and H^1 error norm for RKEM and FEM is given in Figs. 11(b) and 12(b).

5.4. Cantilever beam problem

Consider a linear elastic cantilever beam with external load P acting on its right end. The cantilever beam has a depth $D1$ and length $L4$ as shown in Fig. 13. Using RKEM, we solve it numerically as a plane strain problem with material properties: Young's modulus $E = 3.0 \times 10^7$ and Poisson's ratio $v = 0.3$. The traction boundary conditions at $x = 0$ and $x = L$ are prescribed according to an exact solution. Three uniformly spatial discretizations, with 85, 297 and 1105 nodes, respectively as shown in Fig. 14(a)–(c) are used for convergence study. A bilinear basis was adopted for FEM and for RKEM as well to generate RKEM interpolants with a cubic B-spline kernel function. For comparison, the numerical results of FEM and RKEM, numerical errors are measured by both L2 norm in displacement and energy norm, which are displayed in Fig. 15(a) and (b), respectively. Based on numerical results, the RKEM solution is more accurate than the FEM solution, especially in derivatives, with comparable computational cost.

In the analysis of almost incompressible materials, locking behavior will be observed in the numerical methods with the pure displacement formulation. In RKPM, however locking behavior is reduced or even avoided by choosing a proper dilation parameter. The beam problem with $v = 0.4999$ is analyzed by FEM, RKEM and RKPM. The comparison among the numerical results by using these different methods for solving the cantilever beam with almost incompressible material is made in a table (see Table 1).

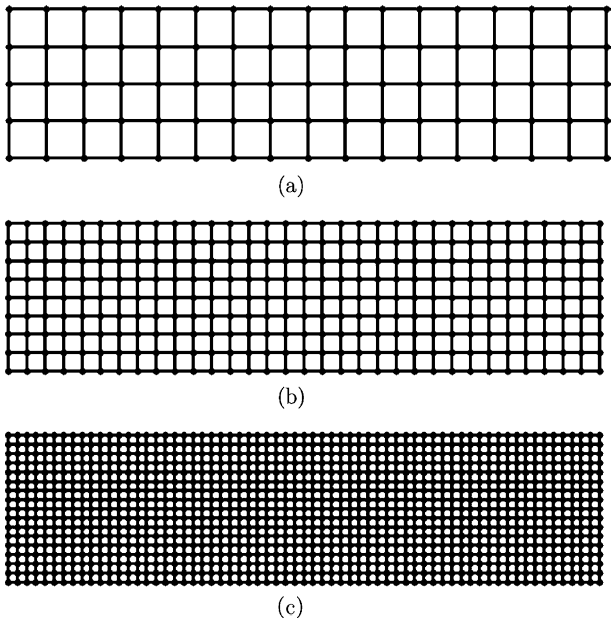

Fig. 14. Model discretizations: (a) spatial discretization I (85 nodes); (b) spatial discretization II (297 nodes); and (c) spatial discretization III (1105 nodes).

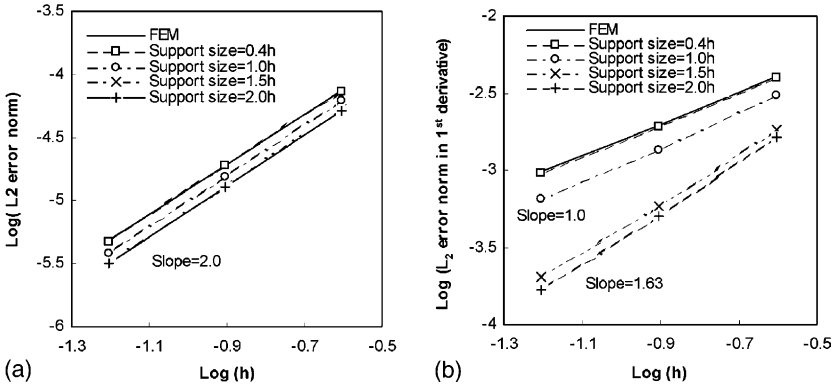

Fig. 15. Error norms for Galerkin solutions of FEM and RKEM: (a) L_2 error norm in displacement for Galerkin solutions; and (b) error norm in energy of Galerkin solutions.

Table 1
Tip deflection accuracy (%) for FEM, RKEM and RKPM in solving beam problem with incompressible material

Methods	5×17 nodes (%)	9×33 nodes (%)	17×65 nodes (%)
FEM	23.6	27.1	27.6
RKEM (with $\rho = 2.0h$)	36.2	66.0	87.7
RKEM (with $\rho = 2.9h$)	72.7	87.3	95.0
RKPM (with $\rho = 2.0h$)	40.8	78.7	89.5
RKPM (with $\rho = 2.9h$)	89.0	95.7	96.6

6. Concluding remarks

This is the first paper in a series devoted to a new class of partition of unities, collectively called RKEM. In the development of RKEM, we remove the smoothness limitation of the finite element method, while at the same time, we maintain the polynomial reproducing property and function interpolation property. Unlike most meshfree interpolants, RKEM interpolants do not need special treatment to enforce Dirichlet boundary conditions. Numerical examples illustrate the satisfactory performance of the new method in solving boundary value problems of higher order differential equations over domains of any dimension, and of arbitrary boundary conditions. This new method also eliminates a major weakness of meshfree interpolants, which lose optimal convergence rates while enforcing Dirichlet boundary conditions when the problem is posed over a multiple dimensional domain and when the polynomial reproducing order is larger than one. In conclusion, unlike most FEM shape functions, RKEM interpolants do not need special treatment in solving high order differential equations, and unlike most meshfree interpolants, an RKEM interpolant can satisfy Dirichlet boundary conditions without any difficulties.

Acknowledgements

This work is made possible by support from NSF under the grant DMI-0115079 to Northwestern University, DMS-0106781 to University of Iowa, and CMS-0239130 to University of California (Berkeley), which are greatly appreciated.

References

[1] I. Babuška, J.T. Oden, J.K. Lee, Mixed-hybrid finite element approximations of second-order elliptic boundary-value problems, Comput. Methods Appl. Mech. Engrg. 11 (1977) 175–206.
[2] T. Belytschko, Y.Y. Lu, L. Gu, Element-free Galerkin methods, Int. J. Numer. Methods Engrg. 37 (1994) 229–256.
[3] T. Belytschko, W.K. Liu, B. Moran, Nonlinear Finite Elements for Continua and Structures, Wiley, England, 2000.
[4] S.C. Brenner, L.R. Scott, The Mathematical Theory of Finite Element Methods, Springer-Verlag, New York, 1994.
[5] J.S. Chen, W. Han, Y. You, X. Meng, A reproducing kernel method with nodal interpolation property, Int. J. Numer. Methods Engrg. 56 (2003) 935–960.
[6] J.S. Chen, H.P. Wang, New boundary condition treatments in meshfree computation of contact problems, Comput. Methods Appl. Mech. Engrg. 187 (2000) 441–468.
[7] J.S. Chen, C. Pan, C.T. Wu, W.K. Liu, Reproducing kernel particle methods for large deformation analysis of nonlinear structures, Comput. Methods Appl. Mech. Engrg. 139 (1996) 195–229.
[8] P.G. Ciarlet, The Finite Element Method for Elliptic Problems, North-Holland, Amsterdam, 1978.
[9] J. Gosz, W.K. Liu, Admissible approximations for essential boundary conditions in the reproducing kernel particle method, Comput. Mech. 19 (1996) 120–135.
[10] F.C. Günther, W.K. Liu, Implementation of boundary conditions for meshless methods, Comput. Methods Appl. Mech. Engrg. 163 (1998) 205–230.
[11] W. Han, X. Meng, Error analysis of the reproducing kernel particle method, Comput. Methods Appl. Mech. Engrg. 190 (2001) 6157–6181.
[12] W. Han, X. Meng, in: Some Studies of the Reproducing Kernel Particle Method, Lecture Notes in Computational Science and Engineering, vol. 26, Springer, 2002, pp. 193–210.
[13] W. Han, G.J. Wagner, W.K. Liu, Convergence analysis of a hierarchical enrichment of Dirichlet boundary condition in a meshfree method, Int. J. Numer. Methods Engrg. 53 (2002) 1323–1336.
[14] S. Hao, W.K. Liu, Revisit of moving particle finite element method, Fifth World Congress on Computational Mechanics, Vienna, Austria, July 7–12, 2002s.
[15] S. Hao, W.K. Liu, Moving particle finite element method with global superconvergence, Int. J. Numer. Methods Engrg. submitted for publication.
[16] S. Hao, H.S. Park, W.K. Liu, Moving particle finite element method, Int. J. Numer. Methods Engrg. 53 (2002) 1937–1958.

[17] I. Kaljevic, S. Saigal, An improved element free Galerkin formulation, Int. J. Numer. Methods Engrg. 40 (1997) 2953–2974.
[18] S. Li, W.K. Liu, Moving least square reproducing kernel method (II) Fourier Analysis, Comput. Methods Appl. Mech. Engrg. 139 (1996) 159–193.
[19] S. Li, W.K. Liu, Meshfree and particle methods and their applications, Appl. Mech. Rev. 55 (2002) 1–34.
[20] S. Li, H. Lu, W. Han, W.K. Liu, Reproducing kernel element, Part II. Globally conforming I^m/C^n hierarchies, Comput. Methods Appl. Mech. Engrg., accepted for publication.
[21] W.K. Liu, S. Jun, S. Li, J. Adee, T. Belytschko, Reproducing kernel particle methods for structural dynamics, Int. J. Numer. Methods Engrg. 38 (1995) 1655–1679.
[22] W.K. Liu, S. Jun, Y.F. Zhang, Reproducing kernel particle methods, Int. J. Numer. Methods Fluids 20 (1995) 1081–1106.
[23] W.K. Liu, S. Li, T. Belytschko, Moving least square reproducing kernel method. Part I: Methodology and convergence, Comput. Methods Appl. Mech. Engrg. 143 (1997) 422–453.
[24] W.K. Liu, R.A. Uras, Y. Chen, Enrichment of the finite element method with the reproducing kernel particle method, J. Appl. Mech., ASME 64 (1997) 861–870.
[25] W.K. Liu, Y. Chen, R.A. Uras, C.T. Chang, Generalized multiple scale reproducing kernel particle methods, Comput. Methods Appl. Mech. Engrg. 139 (1996) 91–158.
[26] H. Lu, J.S. Chen, in: Adaptive meshfree particle method, Lecture Notes in Computational Science and Engineering, vol. 26, Springer, 2002, pp. 251–267.
[27] H. Lu, W.K. Liu, J.S. Chen, J. Cao, Consistent smoothing technique and treatment of material discontinuity in the reproducing kernel element, Int. J. Numer. Methods Engrg., submitted for publication.
[28] H.H. Rachford Jr., M.F. Wheeler, An H^{-1}-Galerkin procedure for the two-point boundary value problem, in: Carl de Boor (Ed.), Mathematical Aspects of Finite Elements in Partial Differential Equations, Academic Press, 1974, pp. 353–382.
[29] G.J. Wagner, W.K. Liu, Hierarchical enrichment for bridging scales and meshfree boundary conditions, Int. J. Numer. Methods Engrg. 50 (2000) 507–524.
[30] G.J. Wagner, W.K. Liu, Application of essential boundary conditions in mesh-free methods: a corrected collocation method, Int. J. Numer. Methods Engrg. 47 (2000) 1367–1379.
[31] L.T. Zhang, G.J. Wagner, W.K. Liu, A parallel meshfree method with boundary enrichment for large-scale CFD, J. Comput. Phys. 176 (2002) 483–506.